Ceria incorporation in sinter-resistant platinum-based catalysts

Michael L. Stone,[1] Melissa C. Cendejas,[2] Alex Persson,[1] Gennaro Liccardo,[1,2] Jacob Smith,[3] Abinash Kumar,[3] Chengshuang Zhou,[1] Evan Gardner, [1] Aisulu Aitbekova,[1] Karen C. Bustillo,[4] Miaofang Chi,[3] Simon R. Bare,[2] Matteo Cargnello[1]*

[1] *Department of Chemical Engineering and SUNCAT Center for Interface Science and Catalysis, Stanford University, 443 via Ortega, Stanford CA, 94304 USA*

[2]*SLAC National Accelerator Laboratory, 2575 Sand Hill Rd, Menlo Park CA, 94025 USA*

[3]*Center for Nanophase Materials Sciences, Oak Ridge National Laboratory, 1 Bethel Valley Rd, Oak Ridge TN, 37830 USA*

[4] *National Center for Electron Microscopy, Molecular Foundry, Lawrence Berkeley National Laboratory, 72 Lawrence Rd, Berkeley CA, 94720 USA*

**Corresponding Author email: mcargnello@stanford.edu*

Keywords: nanocasting, emission control, platinum nanoparticles, thermal stability, hydrocarbon oxidation, catalyst synthesis

Abstract

Platinum group metals (PGM) are widely used for exhaust emission abatement. Sintering during the high-temperature emission control conditions decreases noble metal utilization efficiency. Efficient use of scarce noble metals requires sinter-resistant catalysts**.** Here we extend an approach to synthesize catalysts consisting of platinum nanoparticles encapsulated in a mixture of cerium and aluminum oxides (Pt@Al_2O_3-CeO_2). We tested the activity of this catalyst toward carbon monoxide, propene, and propane oxidation chosen as model oxidation reactions for emission control catalysts. Pt@Al_2O_3-CeO_2 catalysts demonstrated similar activity and stability upon aging as the comparison system without ceria, Pt@Al_2O_3, while maintaining small Pt nanoparticles and ceria crystallites. Additionally, we studied the influence of various thermal treatments on CO oxidation activity and determined that a steam treatment can activate low temperature CO oxidation activity of Pt@Al_2O_3-CeO_2. STEM-EDS analysis revealed that thermal treatments led to the co-location of Pt and CeO_2 and temperature programmed-reduction analysis revealed that the steam treatment specifically enhanced CO oxidation activity through surface reduction of the CeO_2. In summary, we demonstrate the versatility of this encapsulation approach to generate mixed metal-oxide supports with improved metal-support interactions without hindering nanoparticle stability.

Introduction

Emission control catalysts play a critical role in the reduction of pollution and greenhouse gasses. Combustion of fuels in the energy and transportation sectors produces carbon monoxide (CO), nitrogen oxide (NO_x), and hydrocarbons (HC), which are poisonous gasses that lead to the formation of acid rain, smog, ozone and global climate change.[1] Emissions catalysts convert these compounds into CO_2, H_2O and N_2.[2] One ubiquitous example of an emission control catalyst is the automotive catalytic converter, or three-way catalyst (TWC).[3] The TWC consists of an alumina washcoat or carrier layer supported on a ceramic monolith. The washcoat composition has been carefully optimized to perform both reduction (NO_x to N_2) and oxidation reactions (CO and HC to CO_2) across a wide range of operating conditions (fuel rich/reducing to fuel lean/oxidizing) and continued performance across the lifetime of the vehicle.[4,5] The washcoat contains platinum group metals (PGM), with Pt and Pd responsible for CO and hydrocarbon oxidation, while Rh plays the critical role of NO_x conversion.[5] Structural promoters (e.g. La, Ba, Ca) maintain the alumina phase and porosity,[6] and chemical promoters (e.g. CeO_2 and $Ce_xZr_{1-x}O_4$) provide oxygen storage capacity and enhanced catalytic activity.[7] Catalytic converters provide a unique design challenge and opportunities for continued improvement. The TWC must be stable during cycling at the high temperatures (> 800°C) that the catalyst experiences during vehicle operation, and it must continue to meet the Clean Air Act emission standards over 150k miles of driving.[8,9] The TWC must also be active at lower temperatures to effectively clean the engine exhaust during the cold-start phase when the engine is initially turned on, a consideration becoming more important with the prevalence of hybrid vehicles.[10] As such, there are opportunities to continue to improve the high temperature stability and low temperature activity of three-way catalysts.

Sintering of PGM is the primary deactivation mechanism of the TWC. High temperatures along with harsh environments (~10% H_2O, alternating oxidative and reductive environments, sulfur impurities)[9] facilitate the agglomeration of PGM nanoparticles from ~3 nm to ~50-100 nm, resulting in a severe decrease in noble metal utilization efficiency.[11] As a result, automotive catalytic converters use excessively high loadings (~10g total) of Pt, Pd and Rh,[12] accounting for 51% of the global demand for PGM.[13] The reduction of sintering in emission control catalysts is an essential area of research to improve the activity of the catalyst over the lifetime of the vehicle, and reduce the consumption of precious metals, which are costly to both the consumer and the environment. Many developments have been made in the synthesis of sinter-resistant PGM catalysts by tuning the metal-support interactions,[14] developing novel support morphologies to isolate and trap nanoparticles,[15-17] or depositing metal oxide overlayers (e.g. via atomic layer deposition) to coat the nanoparticles.[18-22] A recent perspective highlighted that these promising strategies often presented tradeoffs between catalyst stability and activity, and could be further improved by increased access to the PGM active sites and increased hydrothermal stability of the support.[23]

Ceria (CeO_2) has been highlighted as a key promoter for the low temperature activity of the TWC.[24] CeO_2, a reducible metal oxide with Ce existing in either Ce(III) or Ce(IV) oxidation state,[25] has the ability to form oxygen vacancies.[26,27] This unique feature of ceria opens an alternative reaction mechanism for CO and hydrocarbon oxidation via reverse oxygen spillover at the metal-ceria interface, wherein oxygen from the ceria can react with CO or HC adsorbed on the metal surface.[28-30] This alternative mechanism provides a rate enhancement and achieves lower temperature combustion. Optimizing the PGM-ceria interface can enhance the catalyst activity.[28,31] This has been demonstrated with Pt, Pd, and Rh,[32] with reactions such as methane,[33] CO,[34] and propene combustion.[35] Interactions between PGM and ceria (and subsequent rate enhancements) can be sensitive to thermal treatments, which can modify the Pt size and morphology, as well as the ceria oxidation state and morphology. Oxidative treatments (e.g. 800 °C, 20 vol. % O_2) can facilitate the dispersion of Pt or Pd to single atoms strongly bound to the CeO_2 oxygen vacancies (or Ce(III) sites).[14,36-39] Reductive treatments (e.g. 250-500 °C, CO or H_2) can transform dispersed Pt single atoms into particles and reduce the ceria surface to form more oxygen vacancies.[31,40-45] Steam treatments (e.g. 750 °C H_2O) can restructure the oxygen vacancies in ceria to activate Pt single atoms.[46] Furthermore, high

temperatures can cause growth of ceria crystallites and a collapse of the porosity of the support, reducing the overall activity of the catalyst.[38,47,48] Several recent works have focused on engineering ceria-containing supports to improve catalyst stability, for example through depositing small ceria crystallites on other oxide supports,[49,50] or developing optimal ceria-alumina formulations.[36,51] Most studies have focused on the stabilization of Pt single atoms on ceria vacancies (Ce(III) species).[14,52] Pt single atoms are desired for maximum Pt utilization (100% metal dispersion)[49] and have shown high activity for the CO oxidation reaction.[37,42,46] However, single atom catalysts are less active for other relevant reactions for emission control applications, such as hydrocarbon (>C2) oxidation, which require larger ensemble sites.[49,53,54] In summary, Pt species in Pt-CeO_2 catalysts exposed to oxidative high temperature conditions have a propensity to sinter into large Pt agglomerates and/or disperse into Pt single atom species. While engineering and optimizing the support has improved the stability of dispersed Pt species, there remains an opportunity to develop a Pt-CeO_2 system that stabilizes platinum nanoparticles.

Our recent study demonstrated an alternative approach to synthesize sinter-resistant Pt and Pt/Pd catalysts.[55] By first encapsulating colloidal PGM particles in a polymer framework, we generated a template to synthesize porous alumina around the particles. The resulting encapsulated Pt in alumina (termed Pt@Al_2O_3) demonstrated similar initial activity as a standard Pt supported on alumina (Pt/Al_2O_3) for the propene combustion reaction. The encapsulation technique, termed "nanocasting", prevented the particles from sintering in hydrothermal, oxidative conditions at 800 °C. The PtPd@Al_2O_3 catalyst was stable up to 1,100 °C, as evidenced by maintained propene combustion activity. Here, we expand upon the previous work to incorporate ceria into the nanocasting approach, demonstrating the stabilization of both platinum and ceria, and we explore the influence of ceria on the activity of the catalyst for propene, propane, and CO oxidation.

Results and Discussion

Nanocasting approach for ceria-containing encapsulated catalysts. We hypothesize that the nanocasting technique can directly synthesize mixed metal oxides by mixing precursors during the preparation. Here, we demonstrate that by first encapsulating platinum particles in a polymer framework (POF), we can then utilize an identical Pt@POF to prepare a variety of support compositions, establishing a versatile synthetic platform to tune metal oxide composition for encapsulated catalysts – an essential feature for multi-functional catalysts such as the three-way catalytic converter. **Figure 1a** summarizes the protocol for encapsulation of platinum nanoparticles in porous mixtures of ceria and alumina. Platinum nanoparticles (NPs) (5.2±0.8 nm) were synthesized using colloidal methods following previously published protocols (**Figure 1b**).[55] The NPs were supported on a melamine-based polymer, termed porous organic framework (POF) (**Figure 1c**). The polymer was chosen for its ease of synthesis, inexpensive precursors, porosity and thermal stability, and was synthesized following published protocols.[56] The platinum NPs were encapsulated in POF by growing an overlayer of POF on the Pt/POF (**Figure 1d**). The 5 nm Pt particles maintained their size throughout the polymer encapsulation (size distributions in **Figure S1**). The Pt encapsulated in POF (Pt@POF) was infiltrated with aluminum nitrate and/or cerium nitrate and calcined for 5 hours at 600 °C to generate platinum encapsulated in metal oxides. The ratio of alumina and ceria can be tuned by varying the ratio of their respective nitrates. After an initial screening, we chose 3:1 Al_2O_3:CeO_2 as a promising molar ratio for propene and propane combustion activity after 800 °C and 900 °C aging (**Figure S2 and S3**). Pt encapsulated in pure Al_2O_3 (Pt@ Al_2O_3) and pure CeO_2 (Pt@ CeO_2) were also synthesized for comparison. The same batch of Pt@POF was used for each catalyst and amounts of nitrates were tuned to maintain 0.5 wt. % Pt loading. X-ray fluorescence (XRF) measurements confirmed similar final Pt weight loadings (0.58±0.002 wt. % Pt@Al_2O_3, 0.49±0.003 wt. % Pt@Al_2O_3-CeO_2, 0.48±0.007 wt.

% Pt@CeO_2). Finally, a platinum-free 3:1 Al_2O_3:CeO_2 support was synthesized following the same polymer-infiltration and calcination process. Pt particles from the same colloidal synthesis were supported on the surface of the nanocasted Al_2O_3-CeO_2 support to generate Pt/Al_2O_3-CeO_2, used as a control material to benchmark the activity and stability of the encapsulated materials.

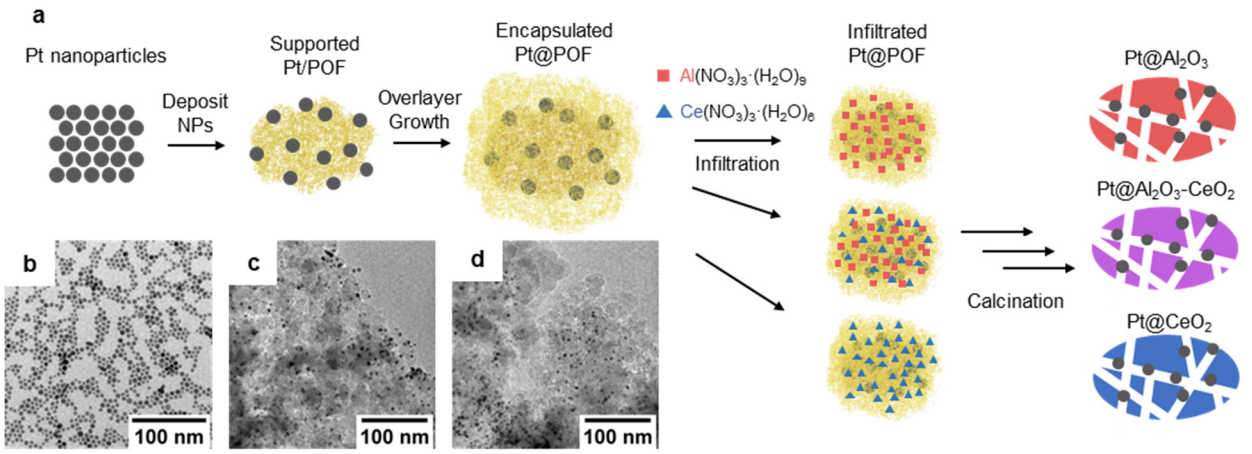

Figure 1. *Nanocasting synthesis schematic*. **a**) overview of the synthesis of nanocasted catalysts. Platinum nanoparticles (NPs) are supported on a melamine-based polymer termed porous organic framework (POF). An additional layer is grown to encapsulate the particles in the polymer (Pt@POF). The same Pt@POF is infiltrated with different amounts of aluminum nitrate and cerium nitrate and subsequently calcined to produce oxides and resulting in the final nanocasted catalysts. Representative TEM images are included of **b)** Pt nanoparticles, **c)** Pt/POF and **d)** Pt@POF.

The as-synthesized encapsulated catalysts were characterized using scanning transmission electron microscope (STEM) imaging and energy dispersive x-ray spectroscopy (EDS) (**Figure 2 a-c**). In the Pt@Al_2O_3 sample, the Pt particles can be easily identified based on the large atomic number Z-contrast between Pt and Al_2O_3 in high-angle annular dark-field (HAADF)-STEM images. The Pt particles are found to be uniformly distributed throughout the interior of the alumina support and maintain their initial particle size of 4.95±1.9 nm (**Figure 2a**, particle size distribution **Figure S4**). Platinum particles were not readily visible in the HAADF-STEM images of Pt@CeO_2 (**Figure 2b**), likely due to a combination of the high atomic number of Ce and the thickness of the ceria support. Instead, the presence of platinum in the Pt@CeO_2 sample was confirmed by XRF (0.48 wt%) and STEM-EDS (**Figure S5**). As dispersion of Pt to single atoms is known to occur on CeO_2,[14] additional STEM imaging was performed on several thin regions of Pt@CeO_2 but did not reveal Pt single atom species (**Figure S6**). Elemental mapping enabled with STEM-EDS was used to locate Pt particles and characterize the distribution of Al and Ce in the Pt@Al_2O_3-CeO_2 sample (**Figure 2 c-f**). A spectrum showing the presence of the Ce_L and Pt_L edges is in **Figure S7**. Pt particle size was found to be maintained after calcination (5.4±2.5 nm, **Figure S4**). Ceria was distributed throughout the sample (**Figure 2f** and lower magnification images included in **Figure S8**). X-ray diffraction (XRD) revealed that the nanocasted alumina was mostly amorphous and the ceria was crystalline (**Figure 2 g**). The Pt@Al_2O_3-CeO_2 support resulted in smaller ceria crystallites (3.8 nm) than the Pt@CeO_2 support (7.8 nm) (size determined by XRD Scherrer equation and supported by STEM images **Figure S9**). Similar crystallite sizes were found whether or not Pt was present during the synthesis of nanocasted Al_2O_3-CeO_2.

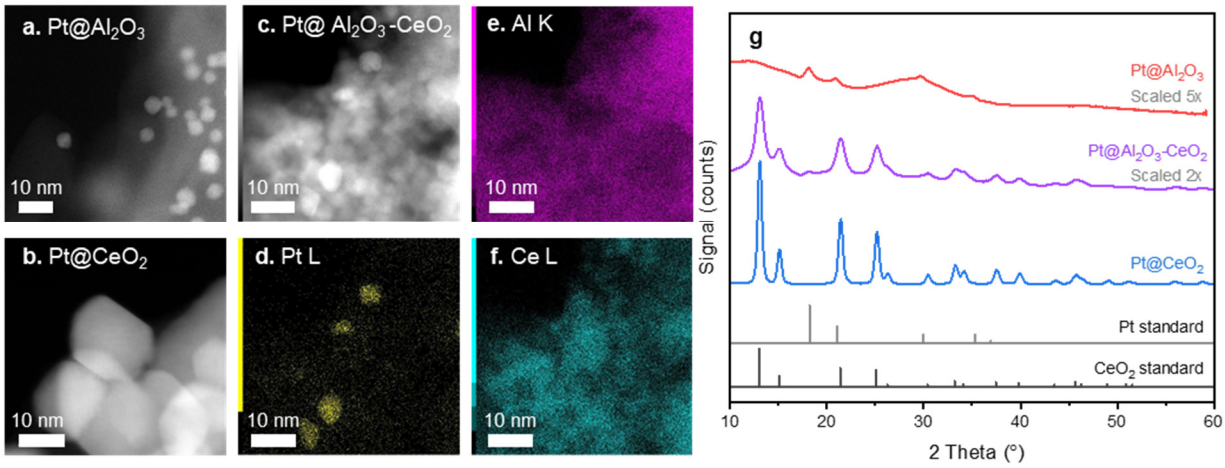

Figure 2. *Characterization of as-synthesized catalysts*. Representative HAADF STEM images of **a)** $Pt@Al_2O_3$, **b)** $Pt@CeO_2$ and **c)** $Pt@Al_2O_3$-CeO_2, along with energy dispersive spectrometry (EDS) elemental maps of Pt L-edge (**d)** Al K-edge (**e**) Ce L-edge (**f**), and **g)** Powder x-ray diffraction (XRD) patterns for $Pt@Al_2O_3$, $Pt@Al_2O_3$-CeO_2, and $Pt@CeO_2$. All peaks can be matched with standard diffraction patterns for Pt and CeO_2 (included for reference).

Reactivity and stability testing. The reactivity of as-synthesized encapsulated and supported catalysts (**Figure 3a**) was evaluated for the complete oxidation of a mixture of CO, propene, and propane. We utilized a testing protocol that simultaneously flowed CO (0.5 vol. %), propene (0.15 vol. %), propane (0.15 vol. %), oxygen (4 vol. %) and water (4.2 vol. %), with argon as the balance. The fresh reactivity of the catalyst was collected after an oxidative and reductive pretreatment and then after aging at 800 °C for 4 h in reaction mixture (**Figure 3b**). 800 °C was selected as the commonly used temperature for accelerated thermal testing of diesel oxidation catalysts.[9] **Figure 3c-e** shows the activity of the fresh $Pt@Al_2O_3$, $Pt@Al_2O_3$-CeO_2, $Pt@CeO_2$ and Pt/Al_2O_3-CeO_2 for CO, C_3H_6, and C_3H_8, respectively. The light-off curves for CO, C_3H_6 and C_3H_8 were collected simultaneously, but have been plotted separately in **Figure 3** for ease of comparison between catalyst samples. We also collected reactivity for the encapsulated catalysts toward each reaction individually (**Figure S10-12)**, which showed similar trends as the reaction performed with the mixture. The fresh catalysts had similar activity for CO and C_3H_6 oxidation, with T50s (temperature required for 50% conversion) in the range of 240-267 °C for CO and 255-281 °C for C_3H_6 oxidation reactions. C_3H_8 combustion showed more dependence on catalyst composition with T50s of 275, 306, 312 and 380 °C for Pt/Al_2O_3-CeO_2, $Pt@CeO_2$, $Pt@Al_2O_3$-CeO_2, and $Pt@Al_2O_3$, respectively (**Table 1**). Notably, ceria-containing catalysts demonstrated propane T50s more than 68 °C lower than the $Pt@Al_2O_3$ catalyst. Light-off curves for the identical set of catalysts after aging in reaction mixture at 800 °C for 4 hours are shown in **Figure 3f-h**. After aging, $Pt@Al_2O_3$ demonstrated stability in line with our previous reports,[55] with a change in 50% conversion temperature (ΔT50) of 12 °C for CO, 2 °C for C_3H_6, and -28 °C for C_3H_8 oxidation. Similarly, $Pt@Al_2O_3$-CeO_2 demonstrated stability with ΔT50s of 8 °C, 4 °C, and 4 °C for CO, C_3H_6, and C_3H_8, respectively. In contrast, the activity of $Pt@CeO_2$ and Pt/Al_2O_3-CeO_2 decreased for all reactions after aging, with ΔT50s ranging from 46 to 114 °C (complete list of T50s in **Table 1)**. In summary, $Pt@CeO_2$ and Pt/Al_2O_3-CeO_2 deactivated while $Pt@Al_2O_3$ and $Pt@Al_2O_3$-CeO_2 maintained almost constant activity. Notably, CO and C_3H_8 showed different sensitivity toward catalyst composition, and aging effects which will be discussed in more detail in later sections.

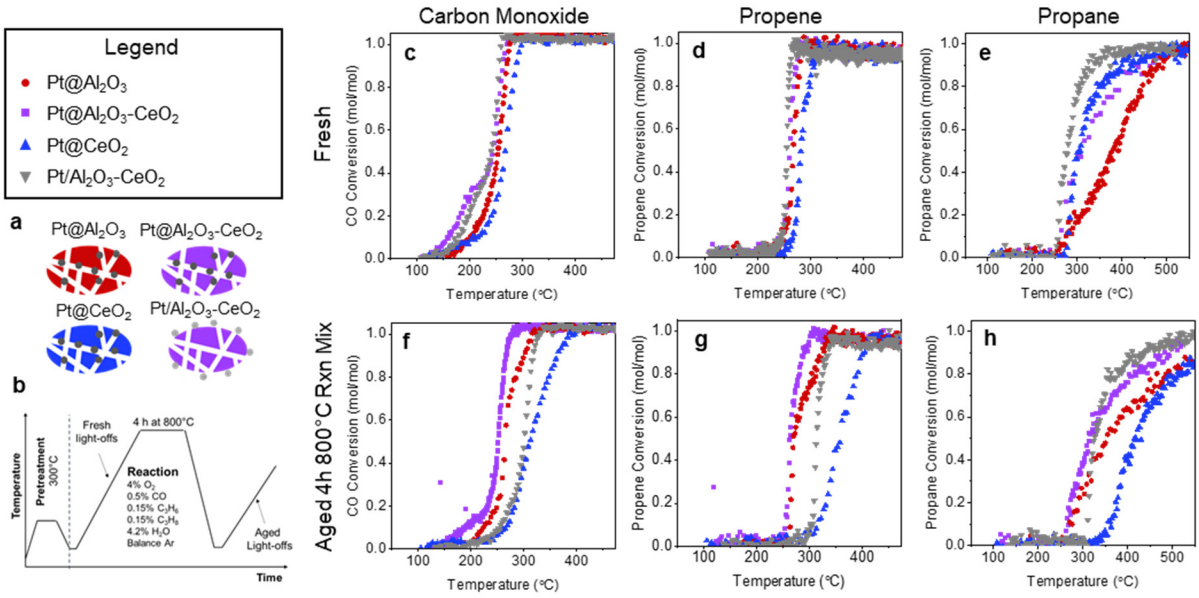

Figure 3. *Reactivity and stability of Pt-Al₂O₃-CeO₂ catalysts*. (**a**) Schematics of the 4 different catalysts and (**b**) temperature profile for the experiments. Top three plots show the light off curves for fresh catalysts reacting with a mixture of CO (**c**), propene (**d**), and propane (**e**). The bottom three plots show the light off curves for catalysts after aging at 800 °C for 4 hours under reaction mixture (4% O_2, 0.5% CO, 0.15% C_3H_6, 0.15% C_3H_8, 4.2% H_2O), separately showing the plots for CO (**f**), propene (**g**), and propane (**h**).

Table 1. *Summary of T50 values for stability experiments shown in **Figure 3***. T50 refers to the temperature at which 50% conversion is achieved. Complete oxidation of CO, propene, and propane oxidation were performed simultaneously, the catalyst was aged at 800°C for 4 hours under reaction mixture, and then the aged light-off curves were collected on the identical catalyst as the fresh light-offs, without removing the material from the reactor.

	Fresh T50 (°C)			**Aged 4h 800 °C Rxn Mix T50 (°C)**			**ΔT50 (°C)**		
Catalyst	*CO*	*Propene*	*Propane*	*CO*	*Propene*	*Propane*	*CO*	*Propene*	*Propane*
Pt@Al₂O₃-CeO₂	244	259	312	252	263	316	8	4	4
Pt@Al₂O₃	253	267	380	265	269	352	12	2	-28
Pt@CeO₂	267	281	306	313	358	420	46	77	114
Pt/Al₂O₃CeO₂	240	255	275	300	313	325	60	58	50

Figure 4 summarizes the TEM characterization of aged Pt@Al_2O_3-CeO_2 and Pt/Al_2O_3-CeO_2. The low-magnification images show that the platinum has clustered in the Pt/Al_2O_3-CeO_2 (**Figure 4b**) but remains dispersed across the support in Pt@Al_2O_3-CeO_2 (**Figure 4j**). The low-magnification EDS images reveal that ceria crystallites remain distributed throughout the alumina after aging in both catalysts (**Figure 4 c-d** and **k-l**). The higher-magnification HAADF-STEM images reveal sintered Pt particles (~100 nm) in the Pt/Al_2O_3-CeO_2 (**Figure 4 e-f**), while smaller (~5nm) Pt particles remain in the Pt@Al_2O_3-CeO_2 (**Figure 4 m-n**). At higher magnification, the bright-field TEM images reveal ceria crystallites (~6 nm) that are in proximity with the Pt particles (**Figure 4q**). The Pt particle size distribution in **Figure 4r** quantitatively summarizes the sintering of Pt/Al_2O_3-CeO_2 and sinter-resistance of Pt@Al_2O_3-CeO_2, with post-aging average Pt particle sizes of 31.9 and 8.8 nm for Pt/Al_2O_3-CeO_2 and Pt@Al_2O_3-CeO_2, respectively.

Analysis of the extended x-ray absorption fine structure (EXAFS) provides information on the average Pt NP size from a significantly larger sample size than the TEM; these data support the NP stability trends discussed above. **Table S 1-2** summarizes the average coordination numbers and the resulting calculated particle sizes of the aged Pt@Al_2O_3-CeO_2 and Pt/Al_2O_3-CeO_2 catalysts (XANES and fitted EXAFS in

Figures S13-S15). A set of Pt-free supports (Al_2O_3, Al_2O_3-CeO_2 and CeO_2) were prepared with identical protocols to evaluate the stability of the supports under thermal aging conditions. **Table 2** summarizes the results of XRD and physisorption characterizations of the supports after aging. Scherrer equation calculations show that Al_2O_3-CeO_2 supports maintain smaller ceria crystallite size than CeO_2 only, after both 800 °C and 900 °C aging conditions (diffraction patterns included in **Figure S16**). Physisorption measurements show the Al_2O_3-CeO_2 support increased surface area after aging while the CeO_2-only support decreased porosity (physisorption isotherms included in **Figure S17-S19**).

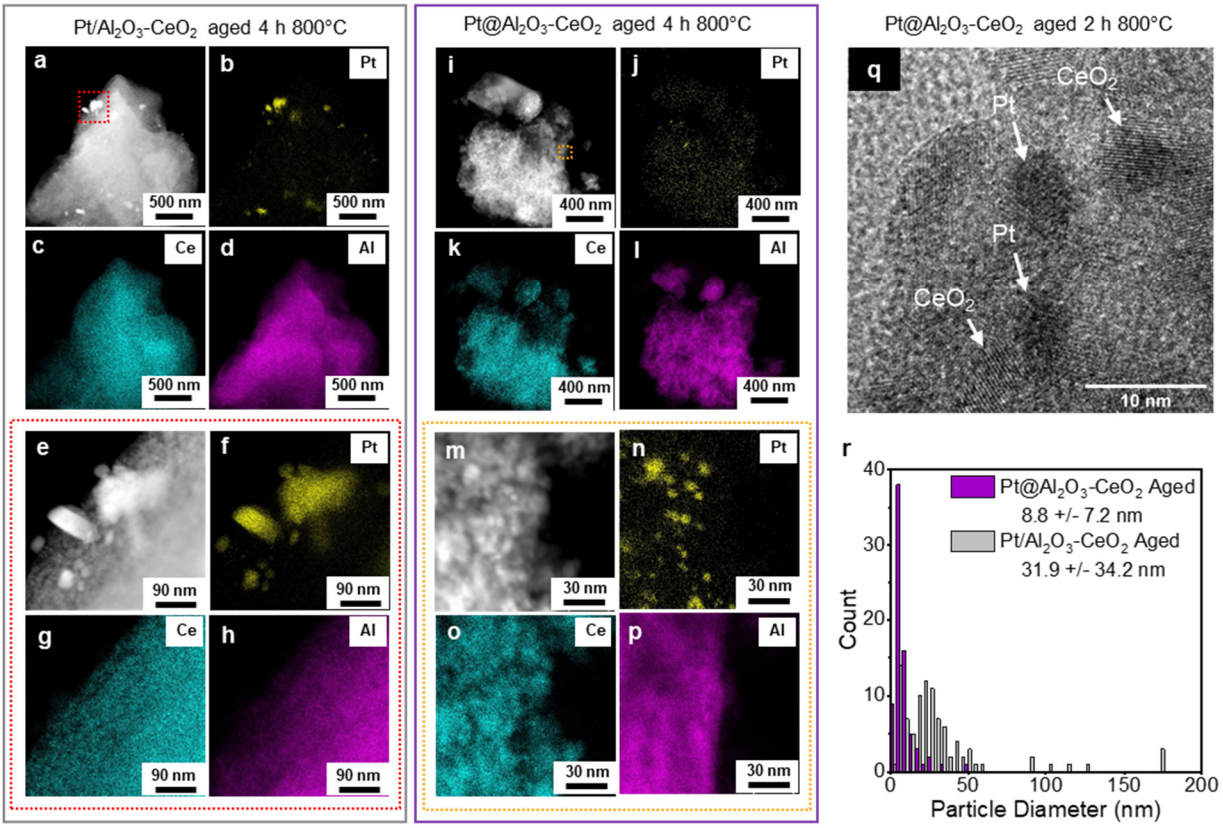

Figure 4. *TEM characterization of Aged Pt-Al_2O_3-CeO_2 catalysts*. **a)** HAADF STEM image of Pt/ Al_2O_3-CeO_2 after aging for 4h at 800 °C in reaction mixture (4% O_2, 0.5% CO, 0.15% C_3H_6, 0.15% C_3H_8, 4.2% H_2O) and EDS elemental maps of **b**) Pt L-edge **c**) Ce L-edge, and **d**) Al K-edge. (**e-h**) HAADF STEM and EDS maps of the region outlined in red in **Fig 4a**. **i)** HAADF STEM image of Pt@Al_2O_3-CeO_2 after 4 h aging at 800 °C in reaction mixture (4% O_2, 0.5% CO, 0.15% C_3H_6, 0.15% C_3H_8, 4.2% H_2O) and EDS elemental maps of **j**) Pt L-edge **k**) Ce L-edge, and **l**) Al K-edge. (**m-p**) HAADF-STEM and EDS maps of the region outlined in orange in **Fig 4i**. **q**) Bright field TEM image of Pt@ Al_2O_3-CeO_2 after aging for 2 h at 800 °C in 3% O_2, 0.15% C_3H_6, 4.2% H_2O. Labelled particles of Pt and CeO_2 were identified based on the lattice spacing. **r**) Particle size distributions for the 4 h 800 °C aged Pt@ Al_2O_3-CeO_2 and Pt/ Al_2O_3-CeO_2.

Table 2. *Characterizing stability of nanocasted supports with XRD and physisorption*. Nanocasted supports were aged in a tube furnace under an atmosphere of 5% O_2, 3% H_2O, balance Ar. Samples for XRD were aged for 1 h at either 800 or 900 °C, with 10 °C/min ramp rates. Samples for physisorption were aged for 4 h at 800 °C in 5% O_2 and 3% H_2O. XRD patterns are included in **Figure S16**. Physisorption isotherms are included in **Figure S17-S19**.

	Ceria crystallite size by XRD Scherrer Equation (nm)			**BET Surface Area**	
Sample	As-synthesized	1 h 800°C	1 h 900°C	As-synthesized	4 h 800°C
Al_2O_3	N/A	N/A	N/A	59 m^2/g	45 m^2/g
Al_2O_3-CeO_2	3.9 nm	5.8 nm	6.5 nm	38 m^2/g	56 m^2/g
CeO_2	7.6 nm	8.8 nm	8.9 nm	18 m^2/g	13 m^2/g

Influence of thermal treatments on CO Oxidation Activity. As-synthesized Pt@Al_2O_3-CeO_2 demonstrated nearly identical propene and CO oxidation activity as Pt@Al_2O_3 (**Figure 3c-d**). Literature precedent has shown that ceria enhances Pt activity for CO oxidation.[34] Also, it has been demonstrated that thermal treatments can significantly influence Pt-CeO_2 interactions, with examples being atom trapping in oxidative conditions,[14,36] oxygen vacancy formation/redistribution in steam treatment,[46] and nanoparticle formation from single atoms under reducing conditions.[40,41] To screen the influence of aging environments on the activity of Pt@Al_2O_3-CeO_2, a simplified reaction and aging protocol was utilized with a reaction mixture of 1 vol. % CO and 1 vol. % O_2 and varying the aging gas composition at 800 °C (**Figure 5a**). The second light-off was used for comparing conditions, due to a slight deactivation between the first and second light-off and maintained activity in subsequent light-offs (**Figure S20**). For each aging treatment, a fresh catalyst was loaded, pretreatment performed, and fresh light-off collected, confirming that the fresh activity was identical across experiments (**Figure S21**). After a given aging treatment, the catalyst was cooled, the gas mixture was switched back to 1% CO and 1% O_2, and two "aged" light-off curves were collected without any intermediate treatment steps (**Figure 5a**). Aging in O_2 or H_2O and O_2 at 800 °C for 1 h or 4 h resulted in identical activity as the fresh catalyst, with T50s within 5 °C of the fresh T50 (297 °C) (**Figure 5b, Table 3)**. 1 h at 800 °C in H_2, H_2O, or Ar enhanced CO oxidation activity with the ΔT50 after aging of -38, -46 and -46 °C, respectively. Activity is further enhanced by treating in H_2O or Ar for longer, with a T50 after 4 h treatment of 215 and 221 °C, respectively. A 4 h steam treatment was selected as the optimal pretreatment to test for the complete set of catalysts and reactions.

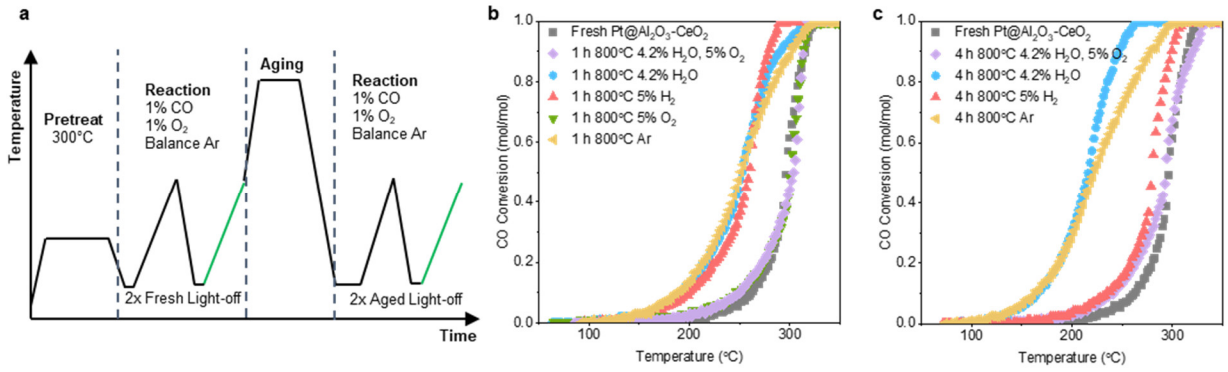

Figure 5. *Influence of aging treatments on CO oxidation with Pt@Al_2O_3-CeO_2 catalyst*. **a)** experimental protocol for CO oxidation and aging. Pretreatment: 300 °C, 30 min 5% O_2, 10 min Ar, 30 min 5% H_2. The second light-off (highlighted green) is the data shown in Figure 5b and c. **b)** Light-off curves for CO oxidation over Pt@Al_2O_3-CeO_2 after pretreatment (Fresh) and after 1 h aging treatments. **c)** Light-off curves for CO oxidation over Pt@Al_2O_3-CeO_2 after pretreatment (Fresh) and after 4 h aging treatments. Note that each aging experiment was performed with a fresh catalyst.

Table 3. Summary of T50 values for CO oxidation over Pt@Al_2O_3-CeO_2 catalyst before and after various thermal treatments shown in **Figure 5**.

Treatment Conditions	T50 (°C)	Delta T50 (°C)
Fresh	297	N/A
1 h 4.2% H_2O	251	-46
1 h 5% H_2	259	-38
1 h 5% O_2	302	5
1 h Ar	251	-46
1 h 5% O_2, 4.2% H_2O	302	5
4 h 5% O_2, 4.2% H_2O	294	-3
4 h 4.2% H_2O	215	-82

4 h Ar	221	-76

The optimized 4 h steam treatment observed by improved CO oxidation activity on $Pt@Al_2O_3$-CeO_2 was then tested on the full set of catalysts ($Pt@Al_2O_3$, $Pt@Al_2O_3$-CeO_2, $Pt@CeO_2$, and Pt/Al_2O_3-CeO_2) and reaction mixture (0.5% CO, 0.15% C_3H_6, 0.15% C_3H_8, 4% O_2 and 4.2% H_2O, balance Ar). Ceria-containing encapsulated catalysts ($Pt@Al_2O_3$-CeO_2 and $Pt@CeO_2$) demonstrated enhanced CO oxidation after steam treatment (**Figure 6 a, d**), with ΔT50s of -83 and -119 °C, respectively (**Table 4**). Steam treatment had a more modest effect on CO oxidation activity of $Pt@Al_2O_3$ or Pt/Al_2O_3-CeO_2, with ΔT50 of -16 and -19 °C, respectively. Steam treatment had an opposite effect on propane combustion activity (**Figure 6 c, f**). T50 for ceria containing catalysts ($Pt@Al_2O_3$-CeO_2, $Pt@CeO_2$, and Pt/Al_2O_3-CeO_2) increased (25, 70, and 38 °C, respectively) and T50 for $Pt@Al_2O_3$ decreased by -66 °C. The propane combustion activity after steam treatment was similar across all catalysts. Steam treatment of ceria-containing catalysts resulted in increased activity for CO oxidation and decreased activity for propane oxidation, indicating differing mechanisms for activating CO and propane in the ceria-containing catalysts. This result may also be related to different structure sensitivity of these reactions after the steam treatment may expose different types of sites on the surface of the metal nanoparticles.[57]

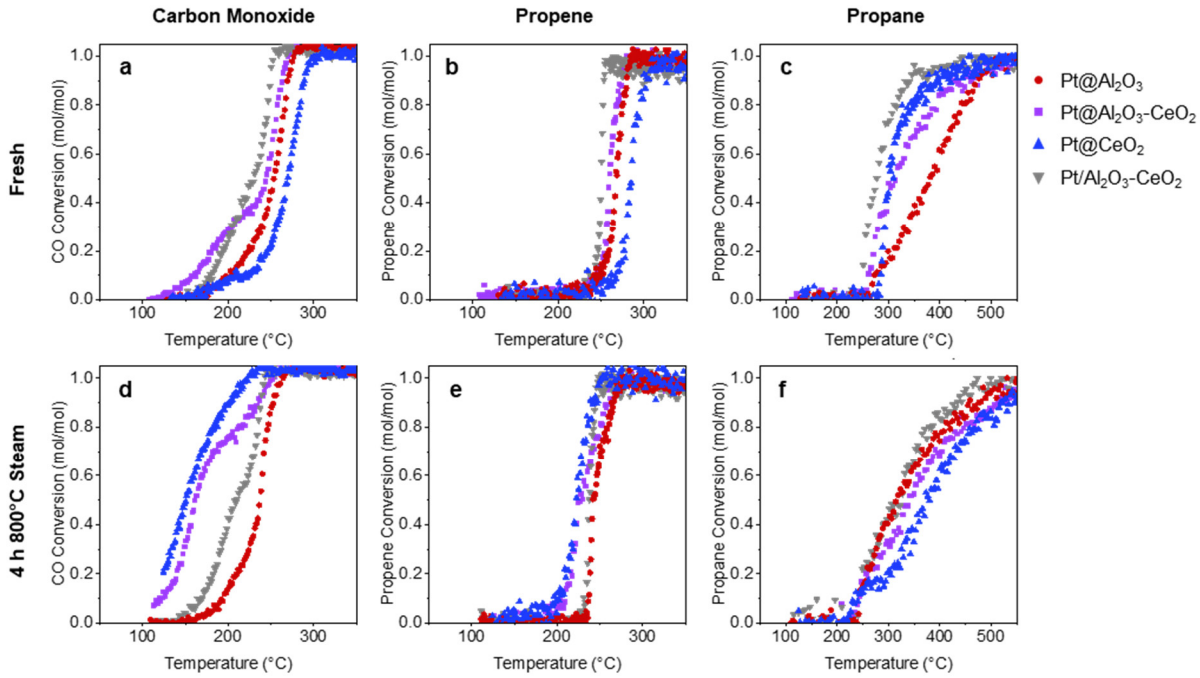

Figure 6. Effect of steam treatment on each catalyst formulation with reaction mixture of CO, propene, and propane. Top three plots show the light off curves for fresh catalysts reacting with a mixture of CO (**a**), propene (**b**), and propane (**c**). The bottom three plots show the light off curves for catalysts after aging at 800 °C for 4 hours under 4.2% H_2O (balance argon), separately showing the plots for CO (**d**), propene (**e**), and propane (**f**). Reaction mixture: 0.5% CO, 0.15% C_3H_6, 0.15% C_3H_8, 4% O_2 and 4.2% H_2O, balance Ar.

Table 4. Summary of T50 values for steam treatment experiments shown in **Figure 6**. T50 refers to the temperature at which 50% conversion is achieved. Complete oxidation of CO, propene, and propane were performed simultaneously, the catalyst was steam treated at 800 °C for 4 hours under 4.2% H_2O/Ar, and then the aged light-off curves were collected on the identical catalyst as the fresh light-offs, without removing the material from the reactor.

	Fresh T50 (°C)			**Steam treated 4h 800 °C T50 (°C)**			**Delta T50 (°C)**		
Catalyst	*CO*	*Propene*	*Propane*	*CO*	*Propene*	*Propane*	*CO*	*Propene*	*Propane*

Pt@Al_2O_3-CeO_2	244	260	313	161	227	338	-83	-33	25
Pt@Al_2O_3	253	268	381	237	242	315	-16	-26	-66
Pt@CeO_2	269	285	309	150	222	379	-119	-63	70
Pt/$Al_2O_3CeO_2$	229	250	277	210	237	315	-19	-13	38

Understanding the changes that occur during steam treatment of Pt@Al_2O_3-CeO_2. Extensive literature on Pt and CeO_2 catalysts have attributed changes to CO and propane oxidation activity to many factors, including changes to the Pt particle size or shape,[34,38,41] changes to the CeO_2 structure,[28] oxidation state,[25,30] or oxygen vacancies,[46] and changes to the support acidity.[58,59] Here, we consider three main hypotheses: 1) increased Pt-CeO_2 interfacial area, 2) change in CeO_2 oxidation state and/or concentration of oxygen vacancies, 3) changes in support surface chemistry.

By the nature of the synthesis, the relative location of ceria, alumina, and platinum cannot be finely controlled, as the cerium and aluminum nitrates are added to the Pt@POF together by infiltration (**Figure 1**). It is known that the activation of Pt by CeO_2 for CO oxidation relies on a direct interface between Pt particles and CeO_2 surface to leverage the reverse oxygen spillover mechanism.[28,34] Using quantitative analysis of STEM-EDS data, we aimed to characterize trends in co-location of Pt and CeO_2 as a function of aging conditions. Several STEM-EDS elemental maps were analyzed for as-synthesized Pt@Al_2O_3-CeO_2, 1 h steam treated Pt@Al_2O_3-CeO_2, 4 h steam treated, 4 h aged (steam + O_2), 4 h steam followed by 1 h O_2 treated, and 4 h aged in reaction mixture (example EDS maps shown in **Figure S22-S26**). The Ce/Al ratio was measured at the location of each Pt nanoparticle (histograms summarized in **Figure S27**). All Pt particles analyzed showed the presence of both Al and Ce in the EDS spectra. Furthermore, the average ratio of Ce/Al increased after 4 h 800 °C treatments. Increased Pt and Ce proximity could result in improved activity, as CO oxidation rates are known to trend with number of Pt-Ce interfacial sites.[34] However, the Ce/Al ratio at the Pt particles location did not trend with activity for CO oxidation, as steam treated and aged (4.2% H_2O, 5% O_2) showed similar increases in Ce/Al ratios, but significantly different activity. Temperature programmed reduction (TPR) experiments comparing the Pt@Al_2O_3-CeO_2 with Pt-free Al_2O_3-CeO_2 support also indicated that the Pt and CeO_2 were in contact in the as-synthesized catalyst (**Figure S28**), further indicating that Pt-CeO_2 proximity is not solely responsible for the trends in activity with steam treatment.

The enhanced activity after steam treatment on Pt@Al_2O_3-CeO_2 was stable after switching to the reaction mixture (1% O_2, 1% CO). Multiple light-offs up to 500 °C showed enhanced activity over the fresh catalyst (**Figure S29**). A steady-state experiment showed that the catalyst stabilized after steam treatment at a rate that was 3.75 times higher than the pre-steam treatment rate (**Figure S30**). However, if the steam-treated catalyst was exposed to oxidative conditions at the higher temperature of 800 °C, the activity decreased to nearly the activity of the fresh catalyst (**Figure 7a**). This experiment, along with the similar activation seen with 1 h steam and 1 h H_2 treatments in **Figure 5b**, supports the hypothesis that steam treatment results in a change in ceria oxidation state. We performed temperature programmed reduction experiments on as-synthesized Pt@Al_2O_3-CeO_2, 4 h 800 °C steam treated Pt@Al_2O_3-CeO_2, and 4 h 800 °C steam treated followed by 1 h 800 °C oxygen treated Pt@Al_2O_3-CeO_2 catalysts (**Figure 7b**). Each TPR experiment was performed on a fresh bed of 100 mg of identical catalyst, and the steam treatment or steam followed by oxygen treatment were performed immediately prior to the TPR. The large decrease in hydrogen consumption between as-synthesized and 4h steam treated catalyst indicates that the ceria was reduced during the steam treatment. Also, the shift of the low temperature peak from 310 °C to 120 °C indicates that the surface of the ceria was more easily reduced after steam treatment, perhaps due to increased Pt-

Ceria interfacial area, as it has been published that the presence of Pt on ceria surface shifts the surface reduction peak to lower temperatures.[40,44] The appearance of a small peak at 190 °C after steam followed by O_2 treatment indicates that the surface of ceria has been oxidized by the high temperature O_2 treatment. This is correlated with a decrease in the activity of the catalyst (evidenced by increased temperature for the light-off curve in panel **a**). Cerium 3d X-ray photoelectron spectroscopy (XPS) of a steam treated (800 °C, 4 h, 3% H_2O/Ar) and an aged sample (800 °C, 4 h, 5% O_2, 3% H_2O, balance Ar) corroborated the TPR results, with the steam treated sample resulting in 24% Ce^{3+} versus 21% Ce^{3+} in the aged sample (**Figure S31** and **Table S3**).

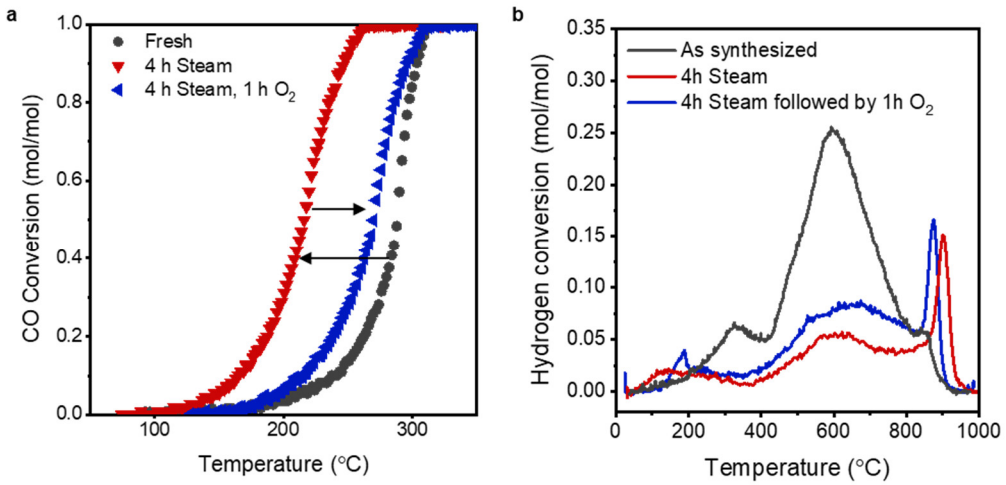

Figure 7. Steam treatment and oxidation of Pt@Al_2O_3-CeO_2 catalyst. **a)** light-off curves for an experiment in which the catalyst was steam treated at 800 °C 4.2% H_2O for 4 hours, then subsequently oxygen treated at 800 °C 5% O_2 for 1 h. Two lightoff curves were collected for the catalyst at each stage, and the second light off curve is plotted. **b.** Temperature programmed reduction (TPR) curves for as synthesized, 4 h 800 °C steam treated, and 4 h 800 °C steam treated followed by 1 h 800 °C O_2 treated. Each TPR experiment was performed on 100 mg of fresh Pt@Al_2O_3-CeO_2 catalyst, and the treatments were performed in-situ immediately prior to TPR.

A temperature-programmed steam treatment experiment revealed that SO_2 was released at 800 °C (**Figure S32**). Sulfur is present in the nanocasted samples as a byproduct of the use of dimethyl sulfoxide solvent during the POF synthesis that breaks down into sulfur-containing species that adsorb on the alumina and ceria surface.[60] The profile for SO_2 release matches published results for thermal decomposition of cerium sulfate.[61] Ceria that is exposed to sulfur is known to readily form cerium sulfate, and cerium sulfate has been shown to increase support acidity.[62] The support acidity could explain the trends in propane combustion activity. It is known that propane combustion activity is increased with increasing support acidity.[58,63,64] Furthermore, recently published work shows that Pt/Al_2O_3 catalysts are enhanced for propane combustion activity by exposure to sulfates.[59] In our work, propane combustion is initially more active in the as-synthesized ceria containing catalyst than the Pt@Al_2O_3. After steam treatment, all catalysts show similar activity, in line with the decomposition of cerium sulfate and balancing of support acidity. However, the release of SO_2 cannot solely explain the trends in CO combustion activity. CO oxidation is further enhanced between 1 h and 4 h steam treatment (despite SO_2 being emitted within the first hour). Also, the reversibility of CO oxidation enhancement seen in steam treatment followed by oxygen treatment indicates that the CO oxidation improvement is not solely due to SO_2 removal. As such, the hypotheses discussed in previous paragraphs (increased Pt-CeO_2 proximity and CeO_2 surface reduction) are likely the main drivers for improved CO oxidation activity after 4 h 800 °C steam treatments.

Conclusions

We demonstrated the synthesis of a nanocasted $Pt@Al_2O_3$-CeO_2 sample, in which 5 nm platinum particles are encapsulated throughout a metal oxide support consisting of amorphous alumina and evenly distributed crystallites of ceria. The composite nanocasted catalyst system stabilized both platinum and ceria crystallites from sintering during aging at 800 °C for 4 hours in oxidative, hydrothermal conditions, maintaining the porosity of the support as well as the activity of the catalyst for simultaneous CO, C_3H_6 and C_3H_8 combustion reactions.

The as-synthesized $Pt@Al_2O_3$-CeO_2 showed similar initial CO and C_3H_6 combustion activity as $Pt@Al_2O_3$, both when the reactants were flowed as a mixture **(Figure 3**) and individually **(Figure S10-S12**). The similar initial CO and C_3H_6 activity indicates that $Pt@Al_2O_3$-CeO_2 and $Pt@Al_2O_3$ have similar availability of Pt sites and that CeO_2 is not participating in CO and C_3H_6 oxidation reactions of as-synthesized catalysts. $Pt@Al_2O_3$-CeO_2 initially demonstrated high C_3H_8 combustion activity versus $Pt@Al_2O_3$, likely due to the presence of acidic cerium sulfate on the catalyst that forms during the calcination step from sulfur impurities in the templating polymer. A 4h 800 °C steam treatment resulted in an increase in the CO oxidation activity of $Pt@Al_2O_3$-CeO_2 catalyst and a decrease in the C_3H_8 combustion activity of $Pt@Al_2O_3$-CeO_2. Three changes were characterized in $Pt@Al_2O_3$-CeO_2 after steam treatment: a release of SO_2 species, a reduction of CeO_2, and co-location of Pt and CeO_2.

After steam treatment, all catalysts showed similar C_3H_8 combustion activity. This was explained by the release of SO_2 from ceria-containing catalysts during the steam treatment. Propane combustion is enhanced by increased support acidity, and it is well known that sulfur-treated ceria has increased acidity. After removing the acidic sulfur species with steam treatment, the ceria no longer impacts the propane combustion activity and $Pt@Al_2O_3$ and $Pt@Al_2O_3$-CeO_2 have similar exposed platinum sites and similar activity.

Steam treatment significantly enhanced the CO oxidation activity of $Pt@Al_2O_3$-CeO_2 while CO oxidation activity $Pt@Al_2O_3$ remained constant after steam treatment. Two main factors were considered for the hydrothermally mediated enhancement of CO oxidation activity in $Pt@Al_2O_3$-CeO_2: proximity of Pt and CeO_2 and oxidation state of CeO_2. STEM-EDS analysis revealed that Pt and CeO_2 are always in proximity in the nanocasted $Pt@Al_2O_3$-CeO_2 catalysts (**Figure S27**). There is some segregation of CeO_2 after long thermal treatments and increased co-location of Pt and CeO_2, although this alone does not explain the trends in CO oxidation activity. TPR experiments (**Figure 7**) and XPS analysis (**Table S3 and Figure S31**) revealed that the ceria surface is reduced slightly by the steam treatment, in comparison with combined steam and oxygen treatments that did not improve CO oxidation activity. Reactivity trends provide additional evidence supporting the characterizations. The importance of Pt-CeO_2 co-location is evident in the steam-activation of the encapsulated $Pt@Al_2O_3$-CeO_2 and $Pt@CeO_2$ while the supported Pt/Al_2O_3-CeO_2 did not demonstrate the same activity enhancement (**Figure 6**). The trends in CO oxidation on $Pt@Al_2O_3$-CeO_2 after thermal treatments in various gas environments (**Figure 5**) support the conclusion the steam reduces the CeO_2. The 1 h treatments in hydrogen and steam resulted in identical activation of $Pt@Al_2O_3$-CeO_2, while no activation occurred while O_2 was present in the aging mixture. Taken together, it is likely the combination of co-location of Pt and CeO_2 and surface reduction of CeO_2 that enhance the CO oxidation activity of $Pt@Al_2O_3$-CeO_2 during steam treatment. Overall, this work demonstrates how this approach leads to mixed oxides supported catalysts with improved activity and high thermal stability for emission control applications.

Supporting information
Contains materials and methods, supporting tables S1-S3 and supporting figures S1-S32

Acknowledgements
This work was supported by the US Department of Energy, Office of Science, Office of Basic Energy Sciences, under contract no. DE-SC0022197. M.L.S. acknowledges support from a TomKat Postdoctoral Fellowship in Sustainable Energy from the TomKat Center at Stanford University. Work at the Molecular Foundry was supported by the Office of Science, Office of Basic Energy Sciences, of the U.S. Department of Energy under Contract No. DE-AC02-05CH11231. The Stanford Synchrotron Radiation Lightsource (SSRL) of SLAC National Accelerator Laboratory is supported by BES under Contract No. DE-AC02-76SF00515. Co-ACCESS is supported by DOE BES Chemical Sciences, Geosciences, and Biosciences Division. We thank the National Science Foundation Division of Materials Research for funding the acquisition of the XPS used in this work (award no. DMR-1828238) and Leah Filardi for assistance with the XPS measurements.

References

1. Choudhary, T., Banerjee, S., and Choudhary, V. (2002). Catalysts for combustion of methane and lower alkanes. Applied Catalysis A: General *234*, 1-23.
2. Kummer, J.T. (1980). Catalysts for automobile emission control. Progress in Energy and Combustion Science *6*, 177-199. https://doi.org/10.1016/0360-1285(80)90006-4.
3. Wang, J., Chen, H., Hu, Z., Yao, M., and Li, Y. (2015). A review on the Pd-based three-way catalyst. Catalysis Reviews *57*, 79-144.
4. Heck, R.M., and Farrauto, R.J. (2001). Automobile exhaust catalysts. Applied Catalysis A: General *221*, 443-457.
5. Funabiki, M., Yamada, T., and Kayano, K. (1991). Auto exhaust catalysts. Catalysis Today *10*, 33-43. https://doi.org/10.1016/0920-5861(91)80072-H.
6. Nortier, P., and Soustelle, M. (1987). Alumina carriers for automotive pollution control. Studies in Surface Science and Catalysis *30*, 275-300.
7. Diwell, A., Rajaram, R., Shaw, H., and Truex, T. (1991). The role of ceria in three-way catalysts. In Studies in Surface Science and Catalysis, (Elsevier), pp. 139-152.
8. Lambert, C.K. (2019). Current state of the art and future needs for automotive exhaust catalysis. Nature Catalysis *2*, 554-557.
9. Rappé, K.G., DiMaggio, C., Pihl, J.A., Theis, J.R., Oh, S.H., Fisher, G.B., Parks, J., Easterling, V.G., Yang, M., and Stewart, M.L. (2019). Aftertreatment protocols for catalyst characterization and performance evaluation: low-temperature oxidation, storage, three-way, and NH 3-SCR catalyst test protocols. Emission Control Science and Technology *5*, 183-214.
10. Gao, J., Tian, G., Sorniotti, A., Karci, A.E., and Di Palo, R. (2019). Review of thermal management of catalytic converters to decrease engine emissions during cold start and warm up. Applied Thermal Engineering *147*, 177-187.
11. Kang, S.B., Lim, J.B., Jo, D., Nam, I.-S., Cho, B.K., Hong, S.B., Kim, C.H., and Oh, S.H. (2017). Ostwald-ripening sintering kinetics of Pd-based three-way catalyst: Importance of initial particle size of Pd. Chemical Engineering Journal *316*, 631-644.
12. Tollefson, J. (2007). Worth its weight in platinum: Booming mineral prices leave car makers scrambling to eke more catalytic performance out of precious metals. Nature *450*, 334-336.
13. Bossi, T., and Gediga, J. (2017). The environmental profile of platinum group metals. Johnson Matthey Technology Review *61*, 111-121.

14. Jones, J., Xiong, H., DeLaRiva, A.T., Peterson, E.J., Pham, H., Challa, S.R., Qi, G., Oh, S., Wiebenga, M.H., Hernández, X.I.P., Wang, Y., and Datye, A.K. (2016). Thermally stable single-atom platinum-on-ceria catalysts via atom trapping. Science *353*, 150-154. doi:10.1126/science.aaf8800.
15. De Rogatis, L., Cargnello, M., Gombac, V., Lorenzut, B., Montini, T., and Fornasiero, P. (2010). Embedded phases: a way to active and stable catalysts. ChemSusChem: Chemistry & Sustainability Energy & Materials *3*, 24-42.
16. Li, G., and Tang, Z. (2014). Noble metal nanoparticle@ metal oxide core/yolk–shell nanostructures as catalysts: recent progress and perspective. Nanoscale *6*, 3995-4011.
17. Yang, X., Li, Q., Lu, E., Wang, Z., Gong, X., Yu, Z., Guo, Y., Wang, L., Guo, Y., and Zhan, W. (2019). Taming the stability of Pd active phases through a compartmentalizing strategy toward nanostructured catalyst supports. Nature communications *10*, 1611.
18. Lu, J., Fu, B., Kung, M.C., Xiao, G., Elam, J.W., Kung, H.H., and Stair, P.C. (2012). Coking-and sintering-resistant palladium catalysts achieved through atomic layer deposition. Science *335*, 1205-1208.
19. Onn, T.M., Arroyo-Ramirez, L., Monai, M., Oh, T.-S., Talati, M., Fornasiero, P., Gorte, R.J., and Khader, M.M. (2016). Modification of Pd/CeO2 catalyst by atomic layer deposition of ZrO2. Applied Catalysis B: Environmental *197*, 280-285.
20. Duan, H., You, R., Xu, S., Li, Z., Qian, K., Cao, T., Huang, W., and Bao, X. (2019). Pentacoordinated Al3+-Stabilized Active Pd Structures on Al2O3-Coated Palladium Catalysts for Methane Combustion. Angewandte Chemie International Edition *58*, 12043-12048.
21. Mao, X., Foucher, A., Stach, E.A., and Gorte, R.J. (2019). A study of support effects for CH 4 and CO oxidation over Pd catalysts on ALD-modified Al 2 O 3. Catalysis Letters *149*, 905-915.
22. Getsoian, A., Theis, J.R., Paxton, W.A., Lance, M.J., and Lambert, C.K. (2019). Remarkable improvement in low temperature performance of model three-way catalysts through solution atomic layer deposition. Nature Catalysis *2*, 614-622.
23. Datye, A.K., and Votsmeier, M. (2020). Opportunities and challenges in the development of advanced materials for emission control catalysts. Nature Materials, 1-11.
24. Trovarelli, A. (1996). Catalytic properties of ceria and CeO2-containing materials. Catalysis Reviews *38*, 439-520.
25. Laachir, A., Perrichon, V., Badri, A., Lamotte, J., Catherine, E., Lavalley, J.C., El Fallah, J., Hilaire, L., Le Normand, F., Quéméré, E., Sauvion, G.N., and Touret, O. (1991). Reduction of CeO2 by hydrogen. Magnetic susceptibility and Fourier-transform infrared, ultraviolet and X-ray photoelectron spectroscopy measurements. Journal of the Chemical Society, Faraday Transactions *87*, 1601-1609. 10.1039/FT9918701601.
26. Campbell, C.T., and Peden, C.H.F. (2005). Oxygen Vacancies and Catalysis on Ceria Surfaces. Science *309*, 713-714. doi:10.1126/science.1113955.
27. Esch, F., Fabris, S., Zhou, L., Montini, T., Africh, C., Fornasiero, P., Comelli, G., and Rosei, R. (2005). Electron Localization Determines Defect Formation on Ceria Substrates. Science *309*, 752-755. doi:10.1126/science.1111568.
28. Vayssilov, G.N., Lykhach, Y., Migani, A., Staudt, T., Petrova, G.P., Tsud, N., Skála, T., Bruix, A., Illas, F., Prince, K.C., Matolı´n, V.r., Neyman, K.M., and Libuda, J. (2011). Support nanostructure boosts oxygen transfer to catalytically active platinum nanoparticles. Nature Materials *10*, 310-315. 10.1038/nmat2976.
29. Bunluesin, T., Putna, E.S., and Gorte, R.J. (1996). A comparison of CO oxidation on ceria-supported Pt, Pd, and Rh. Catalysis Letters *41*, 1-5. 10.1007/BF00811703.
30. Kopelent, R., van Bokhoven, J.A., Szlachetko, J., Edebeli, J., Paun, C., Nachtegaal, M., and Safonova, O.V. (2015). Catalytically active and spectator Ce3+ in ceria-supported metal catalysts. Angewandte Chemie *127*, 8852-8855.
31. Pereira-Hernández, X.I., DeLaRiva, A., Muravev, V., Kunwar, D., Xiong, H., Sudduth, B., Engelhard, M., Kovarik, L., Hensen, E.J.M., Wang, Y., and Datye, A.K. (2019). Tuning Pt-CeO2

interactions by high-temperature vapor-phase synthesis for improved reducibility of lattice oxygen. Nature Communications *10*, 1358. 10.1038/s41467-019-09308-5.
32. Harrison, B., Diwell, A., and Hallett, C. (1988). Promoting platinum metals by ceria. Platinum Metals Review *32*, 73-83.
33. Cargnello, M., Jaén, J.J.D., Garrido, J.C.H., Bakhmutsky, K., Montini, T., Gámez, J.J.C., Gorte, R.J., and Fornasiero, P. (2012). Exceptional Activity for Methane Combustion over Modular Pd@CeO₂ Subunits on Functionalized Al₂O₃. Science *337*, 713-717. doi:10.1126/science.1222887.
34. Cargnello, M., Doan-Nguyen, V.V.T., Gordon, T.R., Diaz, R.E., Stach, E.A., Gorte, R.J., Fornasiero, P., and Murray, C.B. (2013). Control of Metal Nanocrystal Size Reveals Metal-Support Interface Role for Ceria Catalysts. Science *341*, 771-773. doi:10.1126/science.1240148.
35. Lang, W., Laing, P., Cheng, Y., Hubbard, C., and Harold, M.P. (2017). Co-oxidation of CO and propylene on Pd/CeO2-ZrO2 and Pd/Al2O3 monolith catalysts: A light-off, kinetics, and mechanistic study. Applied Catalysis B: Environmental *218*, 430-442. https://doi.org/10.1016/j.apcatb.2017.06.064.
36. Pham, H.N., DeLaRiva, A., Peterson, E.J., Alcala, R., Khivantsev, K., Szanyi, J., Li, X.S., Jiang, D., Huang, W., Sun, Y., Tran, P., Do, Q., DiMaggio, C.L., Wang, Y., and Datye, A.K. (2022). Designing Ceria/Alumina for Efficient Trapping of Platinum Single Atoms. ACS Sustainable Chemistry & Engineering *10*, 7603-7612. 10.1021/acssuschemeng.2c01380.
37. Hill, A.J., Seo, C.Y., Chen, X., Bhat, A., Fisher, G.B., Lenert, A., and Schwank, J.W. (2020). Thermally Induced Restructuring of Pd@CeO2 and Pd@SiO2 Nanoparticles as a Strategy for Enhancing Low-Temperature Catalytic Activity. ACS Catalysis *10*, 1731-1741. 10.1021/acscatal.9b05224.
38. Hill, A.J., Fisher, G.B., Lenert, A., and Schwank, J.W. (2022). Intermediate temperature exposure regenerates performance and active site dispersion in sintered Pd–CeO2 catalysts. Journal of Catalysis *415*, 186-199. https://doi.org/10.1016/j.jcat.2022.10.010.
39. Kunwar, D., Zhou, S., DeLaRiva, A., Peterson, E.J., Xiong, H., Pereira-Hernández, X.I., Purdy, S.C., ter Veen, R., Brongersma, H.H., Miller, J.T., Hashiguchi, H., Kovarik, L., Lin, S., Guo, H., Wang, Y., and Datye, A.K. (2019). Stabilizing High Metal Loadings of Thermally Stable Platinum Single Atoms on an Industrial Catalyst Support. ACS Catalysis *9*, 3978-3990. 10.1021/acscatal.8b04885.
40. Jan, A., Shin, J., Ahn, J., Yang, S., Yoon, K.J., Son, J.-W., Kim, H., Lee, J.-H., and Ji, H.-I. (2019). Promotion of Pt/CeO2 catalyst by hydrogen treatment for low-temperature CO oxidation. RSC Advances *9*, 27002-27012. 10.1039/C9RA05965B.
41. Gänzler, A.M., Casapu, M., Vernoux, P., Loridant, S., Cadete Santos Aires, F.J., Epicier, T., Betz, B., Hoyer, R., and Grunwaldt, J.-D. (2017). Tuning the Structure of Platinum Particles on Ceria In Situ for Enhancing the Catalytic Performance of Exhaust Gas Catalysts. Angewandte Chemie International Edition *56*, 13078-13082. https://doi.org/10.1002/anie.201707842.
42. Gatla, S., Aubert, D., Agostini, G., Mathon, O., Pascarelli, S., Lunkenbein, T., Willinger, M.G., and Kaper, H. (2016). Room-Temperature CO Oxidation Catalyst: Low-Temperature Metal–Support Interaction between Platinum Nanoparticles and Nanosized Ceria. ACS Catalysis *6*, 6151-6155. 10.1021/acscatal.6b00677.
43. Gao, Y., Wang, W., Chang, S., and Huang, W. (2013). Morphology Effect of CeO2 Support in the Preparation, Metal–Support Interaction, and Catalytic Performance of Pt/CeO2 Catalysts. ChemCatChem *5*, 3610-3620. https://doi.org/10.1002/cctc.201300709.
44. Lee, J., Ryou, Y., Chan, X., Kim, T.J., and Kim, D.H. (2016). How Pt Interacts with CeO2 under the Reducing and Oxidizing Environments at Elevated Temperature: The Origin of Improved Thermal Stability of Pt/CeO2 Compared to CeO2. The Journal of Physical Chemistry C *120*, 25870-25879. 10.1021/acs.jpcc.6b08656.

45. Hatanaka, M., Takahashi, N., Takahashi, N., Tanabe, T., Nagai, Y., Suda, A., and Shinjoh, H. (2009). Reversible changes in the Pt oxidation state and nanostructure on a ceria-based supported Pt. Journal of Catalysis *266*, 182-190.
46. Nie, L., Mei, D., Xiong, H., Peng, B., Ren, Z., Hernandez, X.I.P., DeLaRiva, A., Wang, M., Engelhard, M.H., Kovarik, L., Datye, A.K., and Wang, Y. (2017). Activation of surface lattice oxygen in single-atom Pt/CeO₂ for low-temperature CO oxidation. Science *358*, 1419-1423. doi:10.1126/science.aao2109.
47. Perrichon, V., Laachir, A., Abouarnadasse, S., Touret, O., and Blanchard, G. (1995). Thermal stability of a high surface area ceria under reducing atmosphere. Applied Catalysis A: General *129*, 69-82. https://doi.org/10.1016/0926-860X(95)00089-5.
48. Alcala, R., DeLaRiva, A., Peterson, E.J., Benavidez, A., Garcia-Vargas, C.E., Jiang, D., Pereira-Hernández, X.I., Brongersma, H.H., Veen, R.t., Staněk, J., Miller, J.T., Wang, Y., and Datye, A. (2021). Atomically Dispersed Dopants for Stabilizing Ceria Surface Area. Applied Catalysis B: Environmental *284*, 119722. https://doi.org/10.1016/j.apcatb.2020.119722.
49. Jeong, H., Kwon, O., Kim, B.-S., Bae, J., Shin, S., Kim, H.-E., Kim, J., and Lee, H. (2020). Highly durable metal ensemble catalysts with full dispersion for automotive applications beyond single-atom catalysts. Nature Catalysis *3*, 368-375. 10.1038/s41929-020-0427-z.
50. Li, X., Pereira-Hernández, X.I., Chen, Y., Xu, J., Zhao, J., Pao, C.-W., Fang, C.-Y., Zeng, J., Wang, Y., Gates, B.C., and Liu, J. (2022). Functional CeOx nanoglues for robust atomically dispersed catalysts. Nature *611*, 284-288. 10.1038/s41586-022-05251-6.
51. Xie, S., Wang, Z., Tan, W., Zhu, Y., Collier, S., Ma, L., Ehrlich, S.N., Xu, P., Yan, Y., Xu, T., Deng, J., and Liu, F. (2021). Highly Active and Stable Palladium Catalysts on Novel Ceria–Alumina Supports for Efficient Oxidation of Carbon Monoxide and Hydrocarbons. Environmental Science & Technology *55*, 7624-7633. 10.1021/acs.est.1c00077.
52. Dvořák, F., Farnesi Camellone, M., Tovt, A., Tran, N.-D., Negreiros, F.R., Vorokhta, M., Skála, T., Matolínová, I., Mysliveček, J., Matolín, V., and Fabris, S. (2016). Creating single-atom Pt-ceria catalysts by surface step decoration. Nature Communications *7*, 10801. 10.1038/ncomms10801.
53. Bae, J., Kim, J., Jeong, H., and Lee, H. (2018). CO oxidation on SnO2 surfaces enhanced by metal doping. Catalysis Science & Technology *8*, 782-789. 10.1039/C7CY02108A.
54. Jeong, H., Lee, G., Kim, B.-S., Bae, J., Han, J.W., and Lee, H. (2018). Fully Dispersed Rh Ensemble Catalyst To Enhance Low-Temperature Activity. Journal of the American Chemical Society *140*, 9558-9565. 10.1021/jacs.8b04613.
55. Aitbekova, A., Zhou, C., Stone, M.L., Lezama-Pacheco, J.S., Yang, A.-C., Hoffman, A.S., Goodman, E.D., Huber, P., Stebbins, J.F., and Bustillo, K.C. (2022). Templated encapsulation of platinum-based catalysts promotes high-temperature stability to 1,100° C. Nature Materials, 1-8.
56. Schwab, M.G., Fassbender, B., Spiess, H.W., Thomas, A., Feng, X., and Müllen, K. (2009). Catalyst-free Preparation of Melamine-Based Microporous Polymer Networks through Schiff Base Chemistry. Journal of the American Chemical Society *131*, 7216-7217. 10.1021/ja902116f.
57. Huang, W., Johnston-Peck, A.C., Wolter, T., Yang, W.-C.D., Xu, L., Oh, J., Reeves, B.A., Zhou, C., Holtz, M.E., and Herzing, A.A. (2021). Steam-created grain boundaries for methane C–H activation in palladium catalysts. Science *373*, 1518-1523.
58. Yang, A.-C., Zhu, H., Li, Y., and Cargnello, M. (2021). Support acidity improves Pt activity in propane combustion in the presence of steam by reducing water coverage on the active sites. ACS Catalysis *11*, 6672-6683.
59. Cen, B., Wang, W., Zhao, P., Liu, C., Chen, J., Lu, J., and Luo, M. (2022). Revealing the Different Roles of Sulfates on Pt/Al2O3 Catalyst for Methane and Propane Combustion. Catalysis Letters *152*, 863-871. 10.1007/s10562-021-03675-9.
60. R. Riscoe, A., Oh, J., and Cargnello, M. (2022). Sulfur-treated TiO2 shows improved alcohol dehydration activity and selectivity. Nanoscale *14*, 2848-2858. 10.1039/D1NR06029E.
61. Luo, T., Vohs, J.M., and Gorte, R.J. (2002). An Examination of Sulfur Poisoning on Pd/Ceria Catalysts. Journal of Catalysis *210*, 397-404. https://doi.org/10.1006/jcat.2002.3689.

62. Song, J.-Y., Chung, S.-H., Kim, M.-S., Seo, M.-g., Lee, Y.-H., Lee, K.-Y., and Kim, J.-S. (2013). The catalytic decomposition of CF4 over Ce/Al2O3 modified by a cerium sulfate precursor. Journal of Molecular Catalysis A: Chemical *370*, 50-55.
63. Ishikawa, A., Komai, S.i., Satsuma, A., Hattori, T., and Murakami, Y. (1994). Solid superacid as the support of a platinum catalyst for low-temperature catalytic combustion. Applied Catalysis A: General *110*, 61-66. https://doi.org/10.1016/0926-860X(94)80105-3.
64. Yazawa, Y., Yoshida, H., and Hattori, T. (2002). The support effect on platinum catalyst under oxidizing atmosphere: improvement in the oxidation-resistance of platinum by the electrophilic property of support materials. Applied Catalysis A: General *237*, 139-148.

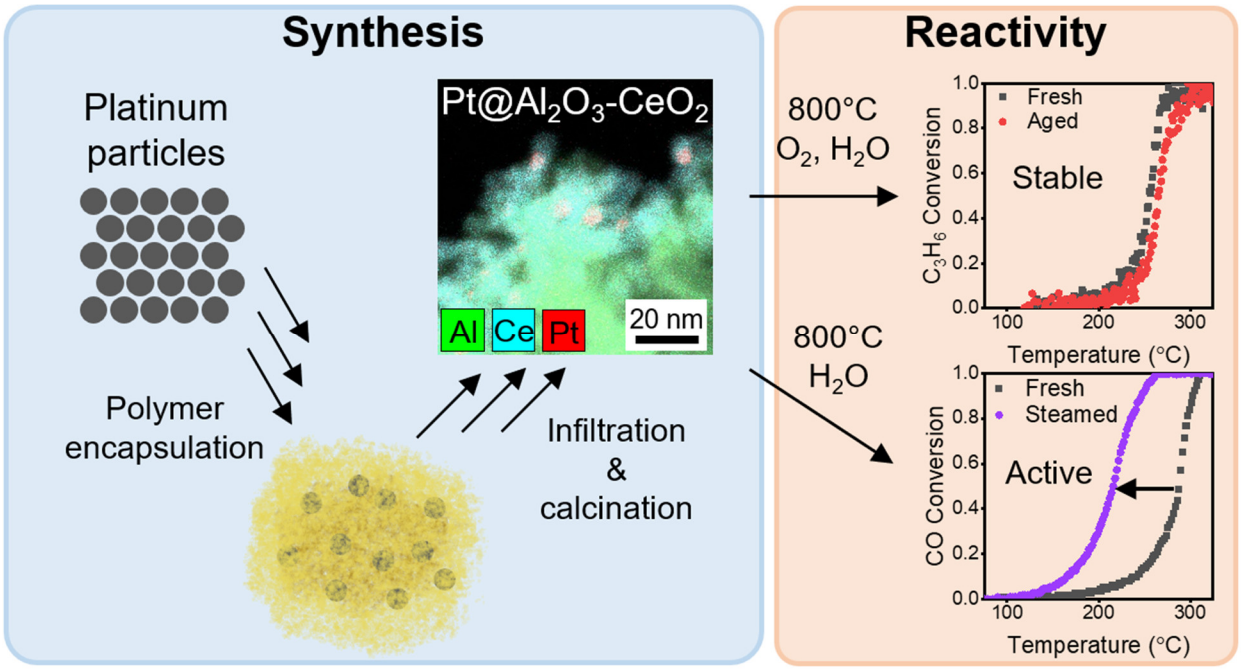
Synthesis
Platinum particles
Polymer encapsulation
Infiltration & calcination
Pt@Al2O3-CeO2
Al
Ce
Pt
20 nm
Reactivity
800°C
O2, H2O
800°C
H2O
Fresh
Aged
Stable
C3H6 Conversion
Temperature (°C)
Fresh
Steamed
Active
CO Conversion
Temperature (°C)